LIMNOLOGY and OCEANOGRAPHY

ASLO

Limnol. Oceanogr. 9999, 2024, 1–12

doi: 10.1002/lno.12624

Phytoplankton biomass responses to a marine heat wave align with altered nitracline depth

Michael R. Landry,[1*] **Alexandra L. Freibott**,[1] **Jennifer L. Beatty**,[1,2] **Karen E. Selph**[3]

[1]Scripps Institution of Oceanography, University of California San Diego, La Jolla, California, USA
[2]Department of Biological Sciences, University of Southern California, Los Angeles, California, USA
[3]Department of Oceanography, University of Hawaii at Manoa, Honolulu, Hawaii, USA

Abstract

The 2014–2015 warm anomaly (aka "the Blob"), the largest of periodic and intensifying marine heat wave (MHW) perturbations in the northeast Pacific, may provide some insight about the future warmer ocean. Here, we use mixed-layer carbon estimates for total phytoplankton, major size classes and functional groups from 45 CalCOFI cruises to: (1) compare 2014–2015 MHW impacts in the southern California Current System to baseline estimates from 2004 to 2013 and (2) to test a space-for-time exchange hypothesis that links biomass structure to variability of nitracline depth (NCD). Seasonal and inshore-offshore analyses from nine stations revealed almost uniform 2°C MHW warming extending 700 km seaward, fourfold to sixfold declines in nitrate concentration and 18-m deeper NCDs. Phytoplankton C decreased 16–21% compared to 45–65% for Chl *a*, with the threefold difference due to altered C : Chl *a*. Among size classes, percent composition of nanoplankton decreased and picophytoplankton increased, driven by higher *Prochlorococcus* biomass, while *Synechococcus* and picoeukaryotes generally declined. Diatom and dinoflagellate C decreased in both onshore and offshore waters. Seasonally, the MHW delayed the normal winter refresh of surface nitrate, resulting in depressed stocks of total phytoplankton and nanoplankton, *Synechococcus* and picoeukaryotes during winter. Consistent with the space-for-time hypothesis, biomass variations for baseline and MHW cruises followed similar (not significantly different) slope relationships to NCD. All biomass components, except *Prochlorococcus*, were negatively related to NCD, and community biomass structure realigned according to regression slopes differences with NCD variability. Empirically derived biomass-NCD relationships could be useful for calibrating models that explore future food-web impacts in this coastal upwelling system.

The southern California Current System (SCCS) is a dynamic region with large onshore-offshore gradients in plankton biomass and composition, as well as substantial mesoscale variability due to fronts, jets, and eddies (Checkley and Barth 2009; Ohman et al. 2013; Taylor and Landry 2018). In 2014–2015, the SCCS along with much of the northeastern Pacific was impacted by a strong and unusually persistent warm-water anomaly (Di Lorenzo and Mantua 2016). Initially termed "the blob" (Bond et al. 2015; Kintisch 2015), recalling an amorphous horror-film creature whose only vulnerability was cold, the 2014–2015 anomaly is now recognized as the largest marine heat wave (MHW) event in the NE Pacific, dating to the earliest documented El Niños (Xu et al. 2021). Ecological impacts in the California Current ranged from poleward shifts in warm-water species distributions to harmful algal blooms and shellfish fisheries closures, reproductive failures of coastal invertebrates, and starvation of seabirds and sea lions (Leising et al. 2015; McCabe et al. 2016; McClatchie et al. 2016; Shanks et al. 2020).

The 2014–2015 MHW first appeared off Alaska in fall 2013, but later separated into two distinct warm water pools off Washington and Baja, Mexico (Kintisch 2015; Peterson et al. 2015). In the SCCS, upper 50-m temperatures reached 4–5°C above seasonal averages, with stratification further intensified by a subsurface salinity minimum at ~ 90 m (Zaba and Rudnick 2016). Other associated physical changes included reduced frequency and magnitude of frontal features (Kahru et al. 2018), usually sites of enhanced vertical

*Correspondence: mlandry@ucsd.edu

Additional Supporting Information may be found in the online version of this article.

Author Contribution Statement: MRL designed the study. ALF and JLB did the microscopical analyses. KES provided flow cytometric analyses. MRL analyzed the data and wrote the manuscript. All authors provided comments and edits.

exchange, productivity and trophic activity. Climate models link the 2014–2015 MHW to increased variability of the Pacific Decadal Oscillation (PDO) and the North Pacific Gyre Oscillation (NPGO) and suggest that similarly intense phenomena with strong thermal stratification and very low nutrients will become more prevalent with climate change (Di Lorenzo and Mantua 2016). To the extent that the 2014–2015 MHW can be viewed as harbinger of future ocean conditions, details of its effects on the pelagic food web base need to be better quantified and understood.

To date, impacts of the 2014–2015 MHW on phytoplankton biomass are mainly known from pigment measurements, which can vary independently of phytoplankton carbon (C) with cell photophysiology, nutrient concentration and taxa (Eppley et al. 1971; Geider 1987). From seasonal cruises along the line P transect, Chl *a* declined 35% in the North Pacific Transition Zone, but that was relatively short lived (Whitney 2015; Yang et al. 2018; Wyatt et al. 2022). Negative Chl *a* anomalies were larger in the southern California Current (23–32°N) than in the northern sector (35–48°N) and larger at normal coastal upwelling sites than offshore (De la Cruz-Orozco et al. 2017; Gómez-Ocampo et al. 2017). Based on relative changes in pigment markers for diatoms and cyanobacteria, Peña et al. (2019) inferred a size structure shift from larger to smaller cells during the 2014–2015 MHW, the expected outcome from enhanced system oligotrophy. Dinoflagellates also increased and possibly replaced diatoms as large phytoplankton dominants in some areas (Du and Peterson 2018), but contributions of eukaryotic phytoplankton were not generally considered with respect to biomass changes. As a consequence, the actual impacts of the 2014–2015 MHW on phytoplankton size and biomass structure remain largely unquantified.

The present investigation expands upon previous pigment-based studies with fully resolved C-based assessments for the total phytoplankton community, for pico, nano, and micro size classes, and for major functional groups of the SCCS region. With the initiation of the CCE-LTER (California Current Ecosystem—Long-Term Ecological Research) Program in 2004, phytoplankton biomass sampling was added to measurements made at a subset of stations that have been regularly sampled on CalCOFI (California Cooperative Ocean Fisheries Investigation) cruises since 1949 (Taylor et al. 2015). Using this fixed-station database extending to 700-km seaward, our first study objective was to compare seasonal and spatial variability of phytoplankton biomass response to the 2014–2015 MHW relative to 2004–2013 baseline trends. The second objective was to evaluate whether the MHW responses followed similar relationships to variability of nitracline depth as in baseline years. This goal derives from a central theme of CCE-LTER process studies (Landry et al. 2009) that seek to understand the mechanistic basis for future conditions in the SCCS with experimental investigations that exploit the system's extensive spatial variability as an analog for temporal change. One prominent hypothesis in this space-for-time approach is the notion that structural changes in the SCCS respond closely to variability of the nitracline depth (Ohman et al. 2013).

Materials and methods

Study sites and sampling

Samples for analyses of phytoplankton biomass and composition were collected off southern California on 45 cruises of the CalCOFI Program over an 11-yr period from November 2004 to November 2015. Collections were made four times per year at nine fixed locations along southern line 90 (Stas. 90.37, 90.53, 90.70, 90.90, and 90.120) extending 68–682 km seaward in the Southern California Bight and northern line 80 (80.55, 80.70, 80.80, and 80.100) extending 32–367 km seaward off Point Conception (Fig. 1). These provide systematically collected environmental and biomass data by season and distance from shore to compare baseline conditions from 2004 to 2013 to those from the 2014–2015 MHW. Supporting Information Fig. S1 shows additional locations of phytoplankton biomass collections from CCE Process cruises over the 2004–2015 period, which are relevant to the supplement plots.

Standard CTD sampling included nutrient samples at all bottle depths (frozen at −20°C for onshore analysis), samples for Chl *a* analysis from the seasurface to below the deep Chl *a* maximum (GF/F filtered, extracted and analyzed by shipboard fluorometry), and samples for phytoplankton community analysis taken from three depths spanning the euphotic zone to the deep Chl *a* maximum. Here, we focus on mixed-layer samples collected generally at 10 m, which was typically the biomass maximum for total phytoplankton C (Taylor et al. 2015). Samples (1–2 mL) for flow cytometry (FCM) analysis were preserved with 0.5% paraformaldehyde and frozen in liquid nitrogen. Samples (500 mL) for epifluorescence (EPI) microscopical analysis were preserved with sequential additions of 260 μL of alkaline Lugol's solution, 10 mL of buffered formalin and 500 μL of sodium thiosulfate (Sherr and Sherr 1993), and stained with the fluorochromes proflavin (1 mL, 0.33% w/v) and DAPI (1 mL, 0.01 mg mL^{-1}). Small volume (SV, 50 mL) subsamples were filtered onto black 0.8-μm polycarbonate filters, the remaining 450 mL (large volume, LV) was concentrated on 8.0-μm filters, and the filters were mounted onto glass slides with type DF immersion oil and frozen at −80°C.

Biomass analyses

Chl *a* values are from samples extracted in 90% acetone for 24 h and measured fluorometrically on shipboard with a Turner AU fluorometer by the acidification method (Holm-Hansen et al. 1965). Community carbon assessments are integrated products from FCM and EPI microscopy as described in by Taylor and Landry (2018). Phytoplankton data for CalCOFI

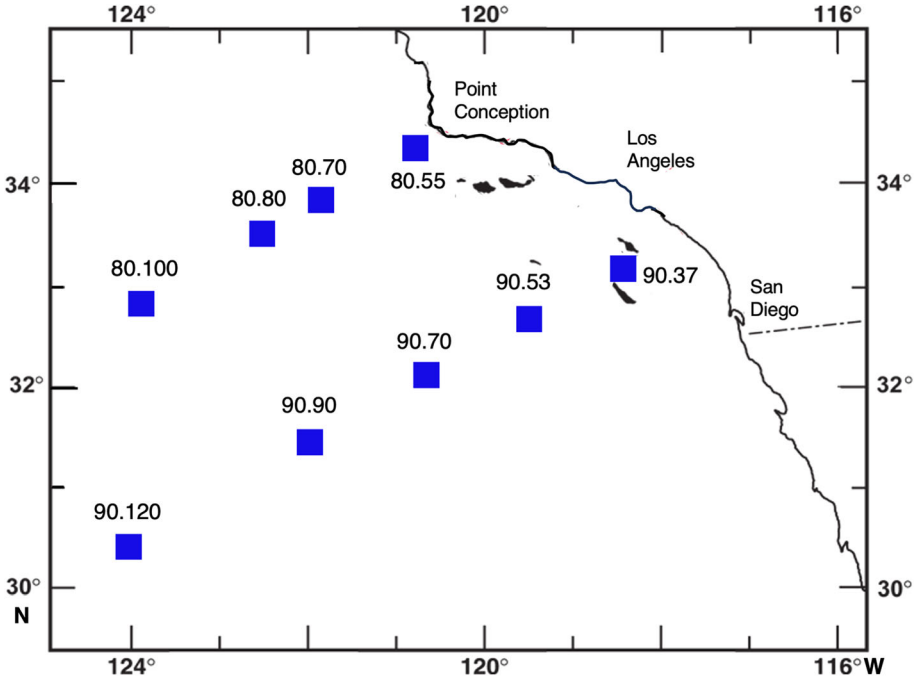

Fig. 1. Sampling stations for phytoplankton community biomass assessments off southern California on quarterly CalCOFI cruises from 2004 to 2015.

cruises are available at the CCE data repository (https://oceaninformatics.ucsd.edu/datazoo/catalogs/ccelter/datasets) as separate abundance and biomass files for Picoplankton (flow cytometry) and Nano-Microplankton (EPI microscopy).

Thawed FCM samples were stained with Hoechst 34442 (1 μg mL^{-1}, final concentration) prior to analysis (Monger and Landry 1993) and analyzed at the SOEST Flow Cytometry Facility using a Beckman-Coulter Altra flow cytometer with a Harvard Apparatus syringe pump to quantify volume sampled and two argon ion lasers tuned to UV (200 mW) and 488 nm (1 W) excitation. Fluorescence signals were collected using filters for Hoechst-bound DNA, phycoerythrin and chlorophyll normalized to internal standards of 0.5-μm UV or yellow–green (YG) polystyrene beads (Polysciences Inc.). Chl *a* containing cells were enumerated as *Prochlorococcus* (Pro), *Synechococcus* (Syn), or phototrophic eukaryotes based on relative size (forward-angle light scatter) and phycoerythrin presence (Syn). Abundance estimates were converted to biomass using mixed-layer estimates of 32 and 101 fg C cell^{-1} for Pro and Syn, respectively (Garrison et al. 2000). Biomass estimates of picoeukaryotes (Peuk, $\leq 2\,\mu$m phototrophic eukaryotes) were determined by first subtracting EPI microscopy abundance estimates for $< 5\,\mu$m eukaryote cells from FCM abundances of eukaryote cells to minimize double counting. The cell abundance difference (assumed cell sizes of 0.8–1.5 μm) was assigned a mean C biomass estimate of 192 fg C cell^{-1}, and this biomass value was combined with the microscopical estimate for 1.5–2.0 μm cells to give total Peuk C.

Microscopical slides were digitally imaged using a Zeiss Axiovert 200M inverted epifluorescence microscope equipped for high-throughput analyses with a motorized focus drive, stage, objective, and filters. Digital images were acquired with a Zeiss AxioCam MRc black and white 8-bit CCD camera. SV samples (50 mL aliquots) were viewed at $\times$630 magnification, and LV samples (450 mL aliquots) were viewed at $\times$200 magnification. A minimum of 20 random positions were imaged for each slide at 5–10 *z*-plane focal depths and for multiple fluorescent channels. The resulting z-stack images were subsequently combined using an extended depth of field algorithm to produce one in-focus false-colored image (Chl a = red, DAPI = blue and FITC = green) for each position, which were analyzed using ImagePro software (Taylor et al. 2015).

Whenever possible, > 300 cells were counted for each slide. Cells were automatically sized and segmented from the background and outlined; user interaction was then required to check each image, split connected cells, outline cells that did not autosegment, and delete artifacts. Phytoplankton were identified by Chl *a* presence (red autofluorescence), generally packaged in defined chloroplasts. Obvious heterotrophic cells with recently consumed prey were excluded. Specific cell categories (diatom, dinoflagellate) were manually assigned, and all cells were grouped into three size categories (Pico, $< 2\,\mu$m; Nano, 2–20 μm; Micro, 20–200 μm) based on lengths of their longest axis. For all size categories, biovolumes (BV; μm^3) were calculated from the length (L) and width (W) measurements of each cell using the geometric formula of a prolate sphere (BV = 0.524 $\times$ LWH), assuming $H = W$. Biomass was calculated as carbon (C; pg cell^{-1}) using the equations of Menden-Deuer and Lessard (2000): C = 0.288 BV$^{0.811}$ for diatoms and C = 0.216 BV$^{0.939}$ for non-diatoms.

Environmental variables

Environmental variables were acquired or computed from data products available at https://calcofi.org/data/oceanographic-data/. For each CTD downcast file, we used temperature, salinity and density measurements at 1-m resolution to determine: (1) mixed-layer depth (MLD), defined as the depth at which sigma-t density first exceeded upper 5-m values by 0.01 kg m^{-3}; (2) mean mixed-layer values of temperature and salinity; and (3) Brunt–Väisälä frequency averaged for upper 60 m (hereafter, N_{60} or buoyancy frequency, 10^{-4} s^{-1}) as a metric of stratification strength (Zaba and Rudnick 2016). From the corresponding CTD bottle data file, we determined: (4) mean nitrate concentration (μmol L^{-1}) for the mixed layer and (5) nitracline depth (NCD, m), the depth where NO_3 first exceeds 1.0 μmol L^{-1}.

Statistical analyses

To test for statistical differences between 2004–2013 baseline and 2014–2015 MHW results for individual seasons (quarterly cruises) and spatial groups (grouped inshore, offshore stations), we used mean log-transformed C biomass values and pair-wise *t* tests (two sided, $\alpha = 0.05$). All seasonal and station results were combined to test for significant slope differences (*t*-test, $\alpha = 0.05$) of log(biomass) vs. nitracline depth relationships for baseline and MHW cruises.

Results

Environmental conditions

Mean environmental conditions for baseline (2004–2013) and MHW (2014–2015) cruises are compared on a seasonal basis (combining locations) in Fig. 2 and between inshore and offshore stations (combining seasons, divided at ~ 200 km offshore) in Table 1. In addition, distributional trends with station distance offshore are provided in Supporting Information Fig. S2 for combined summer–fall cruises, the seasons with warmer more-stratified water and lowest mixed-layer nutrients (Fig. 2), compared to winter–spring cruises.

Mixed-layer temperatures were almost uniformly 2°C warmer across the region during 2014–2015 compared to baseline years, but salinity differences were insignificant (Fig. 2; Supporting Information Fig. S2; Table 1). Stratification strength in the upper 60 m (N_{60}) was generally higher during 2014–2015, but only significantly so during spring cruises over all stations and for Inshore stations over all seasons (Fig. 2; Table 1). However, N_{60} differences would also have been significant for summer cruises for a one-sided test of enhanced stratification during

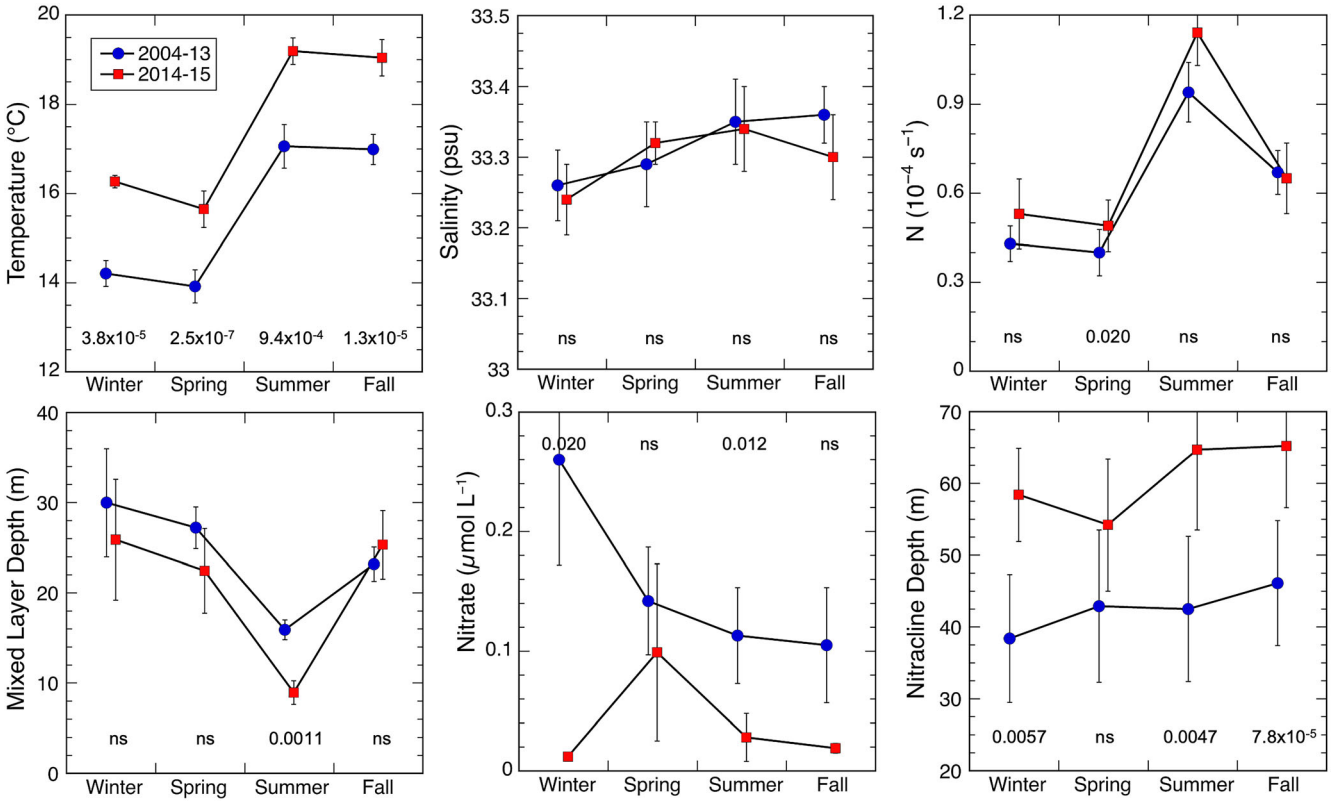

Fig. 2. Mean environmental conditions in the study region as a function of seasons sampled quarterly during 2004–2013 baseline and 2014–2015 cruises. Temperature, salinity and nitrate are mixed-layer values. N_{60} is Brunt–Väisälä (buoyancy) frequency averaged over the upper 60 m. Numbers are *p* values for significant differences; ns, not significant. Uncertainties are standard errors of mean values.

Table 1. Mean (± SEM) environmental conditions and phytoplankton biomass at Inshore (90.37, 90.53, 80.55, 80.70) and Offshore (90.70, 90.90, 90.120, 80.80, 80.100) stations during 2004–2013 baseline and 2014–2015 cruises. Data are all seasons. Units for chlorophyll *a* (Chl *a*) and carbon (C) biomass values are μg L^{-1}. *p* Values indicate significant differences between baseline and 2014–2015; ns = not significant at $p = 0.05$. MLD, mixed layer depth; N_{60}, Brunt–Väisälä buoyancy frequency; Phyto C, total phytoplankton carbon; C : Chl *a*, Phyto C : Chl *a*; Pico, Nano, and Micro are < 2, 2–20, and > 20-μm phytoplankton cells, respectively; %Pico, %Nano, and %Micro C are percent size-class contributions to Phyto C; Pro, *Prochlorococcus*; Syn, *Synechococcus*; Peuk, picoeukaryote; Dino, dinoflagellate.

Variable	2004–2013 Inshore	2014–2015 Inshore	*p* Value	2004–2013 Offshore	2014–15 Offshore	*p* Value
Temp (°C)	15.1 ± 0.5	17.2 ± 0.5	1.0×10^{-6}	15.9 ± 0.4	17.8 ± 0.4	6.0×10^{-13}
Salinity (psu)	33.4 ± 0.04	33.4 ± 0.03	ns	33.2 ± 0.02	33.2 ± 0.03	ns
Nitrate (μmol L^{-1})	0.27 ± 0.05	0.07 ± 0.04	0.0056	0.06 ± 0.02	0.01 ± 0.00	0.0041
MLD (m)	18.1 ± 1.4	14.8 ± 2.2	ns	28.8 ± 2.8	25.4 ± 3.8	ns
Nitracline (m)	19.5 ± 2.7	38.2 ± 3.4	5.1×10^{-6}	60.9 ± 5.1	78.6 ± 4.4	2.4×10^{-4}
N_{60} (10^{-4} s^{-1})	0.83 ± 0.07	0.98 ± 0.08	0.041	0.54 ± 0.05	0.61 ± 0.08	ns
Chl *a*	1.25 ± 0.03	0.44 ± 0.10	0.0093	0.28 ± 0.03	0.15 ± 0.02	1.6×10^{-4}
Phyto C	35.9 ± 3.9	28.2 ± 3.3	ns	15.8 ± 1.2	13.2 ± 1.0	ns
C : Chl *a*	48.2 ± 4.4	76.4 ± 7.7	3.9×10^{-4}	69.8 ± 5.6	96.9 ± 6.9	5.2×10^{-4}
Pico C	8.3 ± 0.6	6.0 ± 0.4	ns	10.6 ± 1.3	6.3 ± 0.4	ns
Nano C	17.4 ± 1.5	12.9 ± 2.1	0.0093	8.5 ± 0.8	5.6 ± 0.5	0.0059
Micro C	10.4 ± 2.6	4.6 ± 0.8	0.043	1.5 ± 0.2	1.4 ± 0.2	ns
%Pico	29.8 ± 2.6	42.9 ± 3.5	2.7×10^{-4}	38.9 ± 1.4	49.6 ± 1.8	1.6×10^{-4}
%Nano	51.6 ± 1.2	43.0 ± 3.1	0.020	53.4 ± 1.3	41.1 ± 1.9	6.0×10^{-5}
%Micro	18.6 ± 3.0	14.1 ± 1.7	ns	7.8 ± 0.7	9.3 ± 1.C	ns
Pro C	0.88 ± 0.16	2.87 ± 0.40	5.3×10^{-4}	2.49 ± 0.15	4.38 ± 0.21	8.0×10^{-6}
Syn C	4.19 ± 0.49	4.86 ± 1.05	ns	2.24 ± 0.32	1.17 ± 0.40	2.3×10^{-4}
Peuk C	3.26 ± 0.34	2.72 ± 0.78	0.021	1.34 ± 0.23	0.59 ± 0.15	0.0014
Diatom C	8.91 ± 2.19	4.61 ± 1.91	0.0025	0.68 ± 0.17	0.22 ± 0.11	2.8×10^{-5}
Dino C	7.57 ± 1.56	2.21 ± 0.36	4.9×10^{-4}	2.80 ± 0.31	1.22 ± 0.27	7.6×10^{-4}

the MHW ($p = 0.036$). While MLDs were generally 2–4 m shallower during 2014–2015 (except for fall), only the summer values differed significantly from baseline (Fig. 2).

Surface nitrate concentrations averaged fourfold to sixfold lower and NCDs were ~ 18 m deeper than baseline values for both inshore and offshore stations in 2014–2015 (Table 1), but the differences were not uniform seasonally or spatially. Seasonally, the MHW extended fall low-nutrient conditions into the winter months of normal maximum surface nitrate (Fig. 2), leading to a significant difference for that season. This collapsed in spring to more seasonally normal (insignificantly different) values of nitrate and NCD in 2014–2015, but significant differences re-established by summer. Spatially, individual offshore stations varied in whether nitrate increased or decreased during winter–spring (Supporting Information Fig. S2). The net effect was a flattening of the variability of nitrate concentration with distance from shore, with 2014–2015 winter–spring values being more like normal summer–fall nitrate concentration while 2104–15 summer–fall concentrations are substantially more reduced (Supporting Information Fig. S2).

Phytoplankton community biomass

Fig. 3 compares mean mixed-layer estimates of phytoplankton community Chl *a*, carbon and C : Chl *a* for seasonal cruises, with mean values and uncertainties for inshore and offshore stations summarized in Table 1. By both C and Chl *a* metrics, phytoplankton biomass declined with distance from shore (Supporting Information Fig. S3), but the magnitudes of spatial, seasonal, and warm-anomaly trends differed substantially between them. On average, 2014–2015 Chl *a* values were ~ 50–60% lower than baseline and significantly different across seasons and locations (Fig. 3; Table 1). In contrast, carbon biomass decreased by ~ 20% on average, significant only for winter cruises (Fig. 3). As a consequence mainly of declining cellular Chl *a*, C : Chl *a* ratios (μg C [μg Chl *a*]$^{-1}$) increased broadly across inshore and offshore stations and for all seasons except spring (Fig 3; Table 1).

Phytoplankton size structure

On average, carbon biomasses of Nano and Micro size classes were lower in 2014–2015 compared to baseline years (Table 1), but the differences are significant for Micro C only at inshore stations and for Nano C at inshore and offshore stations and for winter and summer seasons (Fig. 4; Table 1). The main MHW effect on Pico C was as a significant increase in relative contribution (%Pico) to total Phyto C, which increased for inshore-offshore sites and all seasons, with corresponding declines in %Nano (Fig. 4; Table 1).

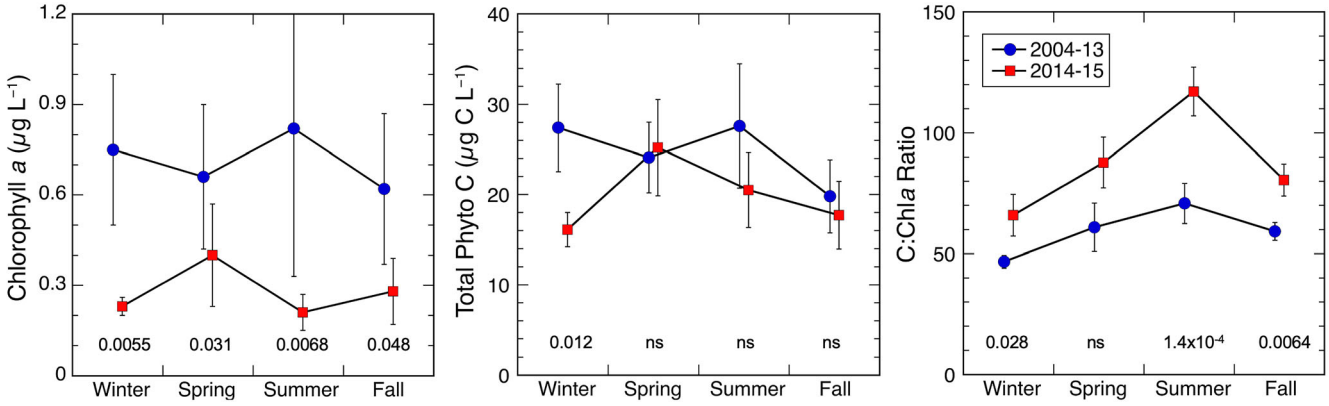

Fig. 3. Mean carbon and Chl *a* estimates of phytoplankton community biomass as function of seasons sampled during 2004–2013 baseline and 2014–2015 cruises. C : Chl *a* is the weight ratio of phytoplankton C to chlorophyll *a*. Numbers are *p* values for significant differences; ns, not significant. Uncertainties are standard errors of mean values.

Group-specific carbon

Within the Pico size fraction, Pro C was consistently and significantly elevated relative to baseline values during 2014–2015, while C estimates for Syn and Peuk were generally reduced, with high variability confounding significance of the seasonal averages among inshore stations (Fig. 5; Supporting Information Fig. S5; Table 1). We do note, however, that Syn C differences for fall and winter seasons and Peuk C differences for fall were only marginally insignificant, and that combining fall–winter cruise data supported lower Syn C ($p = 0.0065$) and Peuk C ($p = 0.0017$) values in 2014–2015. On average, Pro C values were 3.3- and 1.8-fold higher than

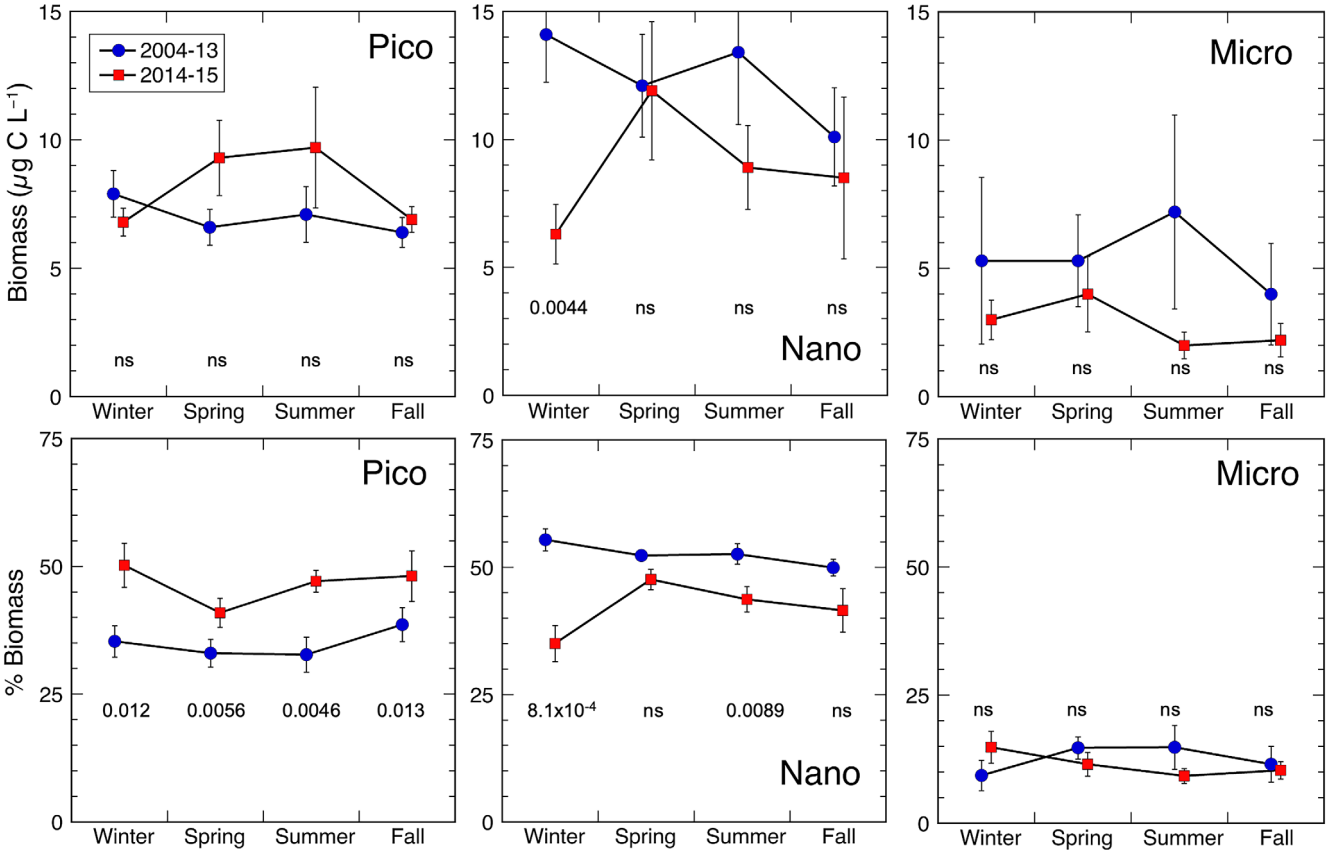

Fig. 4. Mean phytoplankton biomass size structure as function of seasons sampled during 2004–2013 baseline and 2014–2015 cruises. Pico: <2 μm cells; Nano: 2–20 μm cells; Micro: > 20 μm cells. Upper panels are carbon biomass; lower panels are percent of total phytoplankton C. Numbers are *p* values for significant differences; ns, not significant. Uncertainties are standard errors of mean values.

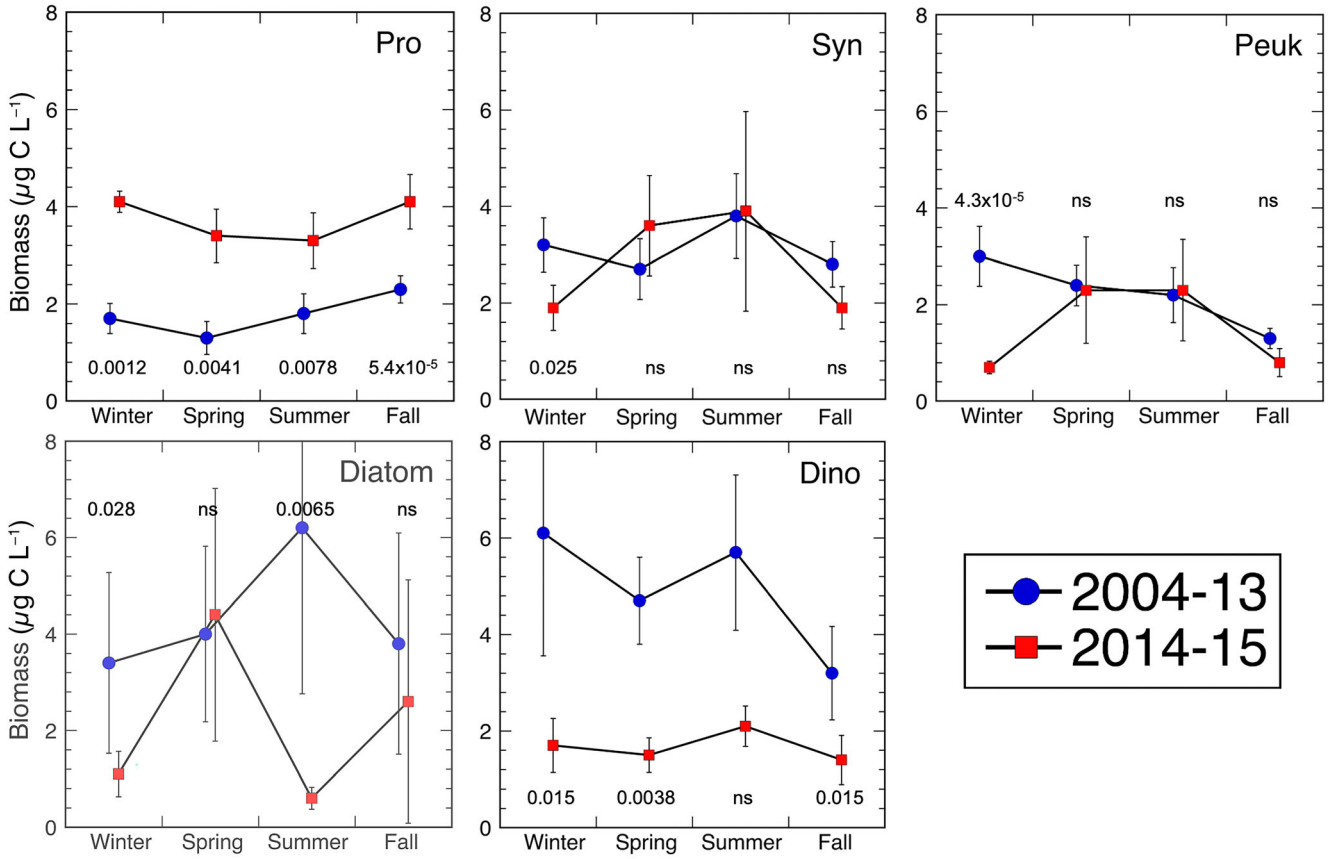

Fig. 5. Mean carbon estimates of phytoplankton groups as function of seasons sampled during 2004–2013 baseline and 2014–2015 cruises. Numbers are *p* values for significant differences; ns, not significant. Uncertainties are standard errors of mean values. Pro, *Prochlorococcus*; Syn, *Synechococcus*; Peuk, picoeukaryote; Dino, dinoflagellate.

baseline at inshore and offshore stations, respectively. Mean Syn C and Peuk C were 48–66% lower than baseline at offshore stations (Table 1).

Diatoms and dinoflagellates are contributors to Micro C but showed stronger responses to the 2014–2015 warming than the Micro fraction overall, exceeding order-of-magnitude declines from 2004 to 2013 baseline values at individual stations (Supporting Information Fig. S6). On average, Diatom C for 2014–2015 was 53% of baseline estimates at inshore stations and 32% of baseline in the offshore, but only the latter was significant (Table 1). Dino C was 29% and 44% of mean baseline values at inshore and offshore stations, respectively, and both were significant. Large variability among the limited number of stations sampled precludes significance for most baseline-MHW comparisons for Diatom C and Dino C, but for all station and seasonal data combined, both were significantly lower in 2014–2015 than baseline years ($p = 0.036$ and 0.00033, respectively).

Biomass-nitracline relationships

To examine relationships between nitracline depth and mixed-layer phytoplankton biomass, we limited the analyses to environmental conditions in which NCD > MLD. This ignores samples with high surface nitrate concentrations, which had highly variable results, ranging from biomass blooms to freshly mixed/upwelled water with very low biomass, and disproportionately affected regression slopes and intercepts due to their large numbers and extreme position in data plots. We also assigned a low value of 0.1 μg C L^{-1} to any data results of zero in order to have valid log-scale numbers in the regressions and data plots. For all biomass categories examined, we found no statistically significant differences in regression slopes between log-transformed biomass and nitracline depth (Fig. 6). That is, for each category, the same regression slope adequately describes the biomass-NCD relationship that applies over all seasonal, spatial, and interannual variability sampled. Among phytoplankton size classes, biomass declines with deepening NCD, but the decrease is sharper (steeper slope) for Micro C and least for Pico C. Response slopes for Nano C and total Phyto C are intermediate.

Among phytoplankton groups, some intercepts and regression lines in Fig. 6 diverge substantially, much of which can be ascribed to samples with zero cell counts (assigned 0.1 μg C L^{-1}).

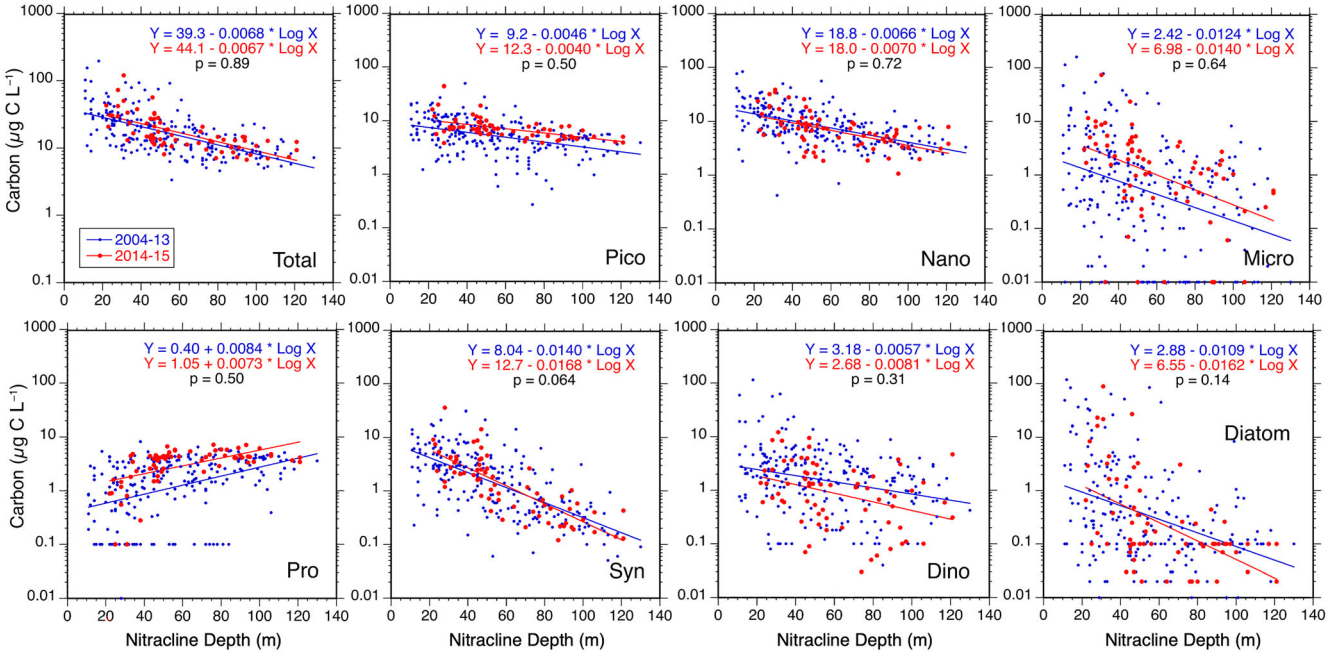

Fig. 6. Relationships of phytoplankton carbon biomass to nitracline depth in the SCCS. Upper panels test regression slope differences between 2004–2013 (blue lines) and 2014–2015 (red lines) for total C and Pico (≤ 2 μm), Nano (2–20 μm), and Micro (> 20 μm) size classes over all seasonal cruises. Lower panels compare slopes for major phytoplankton groups: Pro, *Prochlorococcus*; Syn, *Synechococcus*; Peuk, picoeukaryote; Dino, dinoflagellate. Values of $p > 0.05$ indicate no significant difference in regression slopes.

As noted for Pro, for example, zero cell counts were relatively common in baseline samples from richer waters, such that including them in the least-squares analysis had the effect of pulling the regression line down to where it poorly fit the data where Pro was actually present. Similarly, samples with zero diatoms were substantially more prevalent in the 2014–2015, pulling that regression line lower compared to baseline years (Fig. 6).

Discussion

Based on semi-continuous glider measurements on along CalCOFI lines 90, 80, and 67 from 2006 to 2015, Zaba and Rudnick (2016) ascribed the 2014–2015 warming to anomalous atmospheric heat flux, enhanced downwelling and weakened winds. The first two created a thermally stratified upper ocean with unusually deep isopycnals (thermocline), and the latter reinforced the elevated sea-surface temperature with weakened upwelling and mixing. For our nine sampled stations, the mixed layer experienced a 2-yr mean anomaly of +2°C extending broadly over seasons and locations up to 700-km seaward (Fig. 2; Supporting Information Fig. S2; Table 1). Consistent with strengthened stratification and depressed thermoclines, we found significantly reduced mixed-layer nitrate concentrations and deeper NCDs in 2014–2015 (Table 1). In the Discussion subsections below, we consider our major findings with respect to: (1) phytoplankton size and taxon responses reported in previous studies of the 2014–2015 MHW; (2) biomass response biases due to C : Chl *a* variability, and (3) phytoplankton biomass relationships to NCD.

Phytoplankton response to the 2014–2015 MHW

Previously reported impacts of the 2014–2015 MHW on phytoplankton biomass extend from the Gulf of Alaska to southern Baja, Mexico. From seasonal cruises along the line P transect from 2012 to 2016, the major decline in surface Chl *a* (35%; Whitney 2015) occurred earlier in 2013–2014 and mainly in the North Pacific Transition Zone rather than iron-limited subpolar waters (Wyatt et al. 2022), with Chl *a* returning to baseline levels by August 2014 (Yang et al. 2018; Peña et al. 2019). Overall, the Chl *a* anomaly for 2014–2016 was slightly positive in the northern California Current (35–48°N) while the southern sector (23–32°N) anomaly was sharply negative, especially for normal coastal upwelling locations (De la Cruz-Orozco et al. 2017; Gómez-Ocampo et al. 2017). Nonetheless, northern waters have provided to date the main evidence of altered community composition during the 2014–2015 MHW. For a shallow upwelling station (60 m deep, 9 km from shore) off Oregon, the composition of larger taxa changed from diatom dominance during normal upwelling years to abundant and diverse dinoflagellates during 2014–2015 (Du and Peterson 2018). On the P line, pigment markers for diatoms decreased and cyanobacteria pigments increased during the summers (June) of 2014–2015, suggesting a size structure shift from larger to smaller phytoplankton and

reduced trophic transfer efficiency due to longer food chains (Peña et al. 2019; Wyatt et al. 2022).

While we cannot speak to changes in group diversity, our SCCS results do not suggest a general MHW shift from diatoms to dinoflagellates in the SCCS. C biomasses of both groups declined (Table 1). For inshore stations, the mean decline of Dino C exceeded that of Diatom C, and the relative declines were opposite offshore. Our results may differ from Du and Peterson (2018) because we sampled further offshore and in less upwelling intensive waters, or because their abundance approach did not account for cell size variability of C biomass. In this regard, we note that diatom chains in the present study were enumerated as the sum of individual (generally nano-sized) cells, which relates better to their advantages as competitors for dissolved nutrients rather than size availability as a food particles for consumers (Taylor et al. 2015). Thus, diatoms are not synonymous in our analyses with the largest (Micro) phytoplankton, which varied differently in MHW response (Figs. 4, 5; Table 1).

The observed change in relative dominance of Pico- and Nano-sized phytoplankton (Fig. 4; Table 1) is a major result of the present study that confirms and quantifies the MHW size shift to smaller cells suggested by Peña et al. (2019). Our results demonstrate additionally, however, that analyses of component populations are not equally indicative of that result. For example, while %Pico contribution to total biomass increased significantly for both onshore and offshore stations and for all seasons, these differences are almost entirely driven by increasing Pro C, because Syn and Peuk C changed insignificantly at inshore stations and declined offshore (Fig. 4; Table 1). Thus, Pro, by itself, exaggerated the Pico response; Syn and Peuk underestimated the Pico response, and even measuring all of them together showed an insignificant Pico C increase, unless determined (as %Pico) relative to total Phyto C.

One previously unobserved finding of the present study is the extension of very low mixed-layer nitrate concentrations from the normal fall minimum into the 2014–2015 winters, the season of highest concentration during baseline years (Fig. 2). This occurred without any substantial differences in the mean seasonal patterns of N_{60} stratification, MLD or NCD. Winter was correspondingly the only season for which significant biomass differences (decreases) relative to baseline were observed for total Phyto, Nano, Syn, and Peuk C (Figs. 3–5). Thus, if the 2014–2015 MHW can be viewed as a preview of future ocean conditions, one expected system-level effect could be a significant delay and overall reduction in the seasonal refresh of euphotic zone nutrients, with wintertime phytoplankton biomass and consumers dependent on the timing of that resource being notably impacted.

Chl *a* exaggerates the heat wave impact on phytoplankton biomass

Phytoplankton cellular Chl *a* and C : Chl *a* ratios are known to vary by an order-of-magnitude or more with light, nutrients, taxonomic composition, and other factors (Eppley et al. 1971; Cullen 1982; Geider 1987). Nonetheless, since Chl *a* is easily measured from shipboard analyses, instrumented drifters and remote sensing, it remains the key variable for reporting phytoplankton biomass and projecting climate change impacts in the oceans. We highlight the C : Chl *a* issue here because it is rare to have a sufficiently large database of comparative C biomass determinations to assess the magnitude of the Chl *a* bias as a biomass metric.

On average, Chl *a* measurements suggest a 65% MHW decline of mixed phytoplankton biomass from baseline values for inshore stations and a 47% decline for offshore stations (Fig. 3; Table 2). The corresponding C decline estimates are 21% and 16%, respectively. From these differences, Chl *a* measurements overestimated the C biomass impact of the 2014–2015 MHW by a factor of 3. C estimates may also have methodological issues from the assumed constancy of C : BV relationships for microscopical analyses and fixed cell C values for flow cytometry populations. Nonetheless, to the extent that those methods were applied consistently in this study,

Table 2. Regression relationships of phytoplankton carbon (C) biomass variables vs. nitracline depth for all 2004–2015 data. Intercepts (*a*) and slopes (*b*) are in the format of $Y = a + b \times \log(\text{biomass}, \mu\text{g C L}^{-1})$ with (95% C.L.) = 95% confidence limits. R, correlation coefficient; p, significance of regression slope; Phyto C, total phytoplankton carbon; Pico, Nano and Micro C are carbon biomasses for < 2, 2–20, and > 20-μm phytoplankton cells, respectively; Pro, *Prochlorococcus*; Syn, *Synechococcus*; Peuk, picoeukaryote; Dino, dinoflagellate.

Biomass	Intercept (95% C.L)	Slope (95% C.L.)	*R*	*p* Value
Phyto C	39.9 (34.7, 45.8)	−0.0068 (−0.0058, −0.0077)	0.63	7.0×10^{-34}
Pico C	9.6 (8.1, 11.2)	−0.0042 (−0.0031, −0.0053)	0.39	2.7×10^{-12}
Nano C	18.7 (15.8, 22.1)	−0.0068 (−0.0056, −0.0079)	0.55	5.0×10^{-25}
Micro C	2.8 (1.7, 4.9)	−0.0122 (−0.0084, −0.0160)	0.35	6.3×10^{-10}
Pro C	0.23 (0.15, 0.38)	+0.0115 (0.0082, 0.0148)	0.37	7.3×10^{-11}
Syn C	8.7 (6.9, 11.1)	−0.0145 (− 0.0129, −0.0162)	0.71	2.9×10^{-46}
Peuk C	3.5 (2.5, 4.9)	−0.0131 (−0.0108, −0.0155)	0.54	3.6×10^{-23}
Diatom C	2.2 (1.3, 3.9)	−0.0187 (−0.0150, −0.0225)	0.50	6.9×10^{-20}
Dino C	3.0 (2.0, 4.5)	−0.0070 (−0.0042, −0.0099)	0.27	2.4×10^{-6}

the relatively modest C decline vs. threefold higher Chl *a* estimates have grossly different implications for projecting MHW impacts on the food web and trophic flows. In that regard, Morrow et al. (2018) compared results for CCE cruises during normal and MHW years and found no significant differences in functional relationships describing zooplankton grazing on > 3-μm Chl *a* or between measurements of C export compared to primary production, mesozooplankton grazing, and fecal pellet or pigment fluxes. They did however observe that primary production rates were significantly lower at similar light levels during the MHW, which they ascribed to reduced nutrient concentrations and altered community composition.

Our mean C : Chl *a* estimates of 48–97 (Table 1) bracket the widely used estimate of 58 from Eppley et al. (1992), with more substantial seasonal, spatial, and event-scale variability in individual samples. While (unmeasured) changes in phytoplankton community composition may have contributed partially to the C : Chl *a* differences, most can be reasonably ascribed to photophysiological adjustments associated with the fourfold to sixfold nitrate decline in 2014–2015 because MLDs, hence mean light levels experienced, were relatively similar between baseline and MHW years (Table 1). In addition, however, shifts in nutritional strategy could have contributed to C : Chl *a* increase if increased oligotrophy selected for mixotrophic forms (Stoecker 1998; Unrein et al. 2014) that rely less on phototrophy and more on phagotrophy to satisfy their cell growth requirements.

Nitracline depth as a space-for-time predictor of biomass variability

Space-for-time exchange is a widely used approach for predicting future trends in ecosystem structure and dynamics from contemporary relationships (Carmack et al. 2014; Bjorkman et al. 2018; Dong et al. 2020; Monteiro et al. 2022). Since its early days, CCE-LTER has operated under the explicit hypothesis that spatial variability can serve as an analog for long-term temporal change, and that has been the central concept for designing CCE studies that exploit natural system variability as a strategy for developing the mechanistic basis for ecosystem forecasting. In that regard, NCD has emerged as a parameter with appropriate range in spatial and interannual variability, strong response to natural climate oscillations (ENSO, PDO), and significant correlation with Chl *a* standing stock (Ohman et al. 2013). While NCD is a proxy for many factors that influence nutrient delivery to the euphotic zone, its variably is more in step with the time scales of community change, as opposed to the more dramatic swings in mixed-layer nitrate, which are often out of phase with biomass blooms and crashes. A recent ecosystem model for the SCCS region has also suggested that depth of the pycnocline and associated nutricline is the leading factor explaining variability in new production and biogeochemical state of the system (Deutsch et al. 2021).

In the present study, mixed-layer C biomasses of the phytoplankton community, three size classes and diverse groups are all shown to vary significantly with NCD (Fig. 6). Consistent with the space-for-time hypothesis, biomass variations associated with the 2014–2015 MHW follow similar (not significantly different) relationships to NCD as in the preceding decade of baseline observations. We do note, however, that high frequencies of zero biomass values for specific taxa like Pro and diatoms affect regression coefficients, which can be a significant constraint in resolving relationships for rarer taxa. Regardless, one can make reasonable predictions of future trends in SCCS phytoplankton biomass based on NCD relationships from the current results, which were re-determined in Table 2 based on all 2004–2015 data. Pro C is the only biomass component that predictably increases with NCD. Size structure changes are also reasonably predicted from the relatively tight size class relationships with non-overlapping confidence limits of regression slopes. Micro C declines most rapidly with NCD, the slope of Pico C decline is a factor of 3 lower, and the decline of Nano C is intermediate. Non-intuitively, Syn and Peuk C decrease with NCD at rates similar to larger Micro-sized cells. Thus, as noted above, the Pico C relation to NCD variability differs substantially from any of the populations (Pro, Syn, Peuk) that comprise the Pico size class. High variability in C biomass assessments for diatoms and dinoflagellates likely precludes their NCD relationships from having much predictive value. It is notable, however, that Dino C declines with NCD at a moderate rate, similar to total Phyto C and Nano C, which reflects the ubiquitous importance of dinoflagellates across productive and oligotrophic ocean systems owing to their diverse lifestyles and widespread mixotrophy. Given that they follow similar biomass-NCD slope relationships, the phytoplankton responses to the 2014–2015 MHW can be interpreted, to first order, as a realignment of community composition that relates to deepening of the NCD.

While biomass-NCD relationships in Table 2 provide testable details for predicting future biomass trends, they have no association with specific mechanisms driving NCD change, which are still poorly resolved. Zaba and Rudnick (2016) noted, for example, that the physical drivers of surface warming and pycnocline depression during the 2014–2015 MHW differed from those that give subsurface warming and significant northward advection during typical El Niño events. Rykaczewski and Dunne (2010) have further suggested that altered circulation and reduced ventilation in the future North Pacific might enrich nitrate source water and result in elevated phytoplankton stocks and productivity in the SCCS compared to current and historical values. Such changes are counterintuitive to the established inverse relationship between temperature and productivity for the SCCS (Rykaczewski and Dunne 2010) but would be entirely compatible with current results presuming that richer nitrate source water would manifest as shallower NCDs. In short, basin-scale processes that will shape the future physical and biogeochemical environment of

the eastern North Pacific are still playing out, and even the direction (positive or negative) of the impacts on nutrient supply and NCD are currently undetermined. Biomass-NCD relationships incorporate much of what we presently know about temporal and spatial biomass variability in the SCCS. They offer a mechanistically neutral approach for predicting future biomass change and could also be useful in informing and calibrating models that can explore more deeply how future changes might alter food webs and ecological services.

Data availability statement

All data are publicly available at data repository websites for the CalCOFI (https://calcofi.org/data/oceanographic-data/) and CCE-LTER Programs (https://oceaninformatics.ucsd.edu/datazoo/catalogs/ccelter/datasets).

References

Bjorkman, A. D., and others. 2018. Plant functional trait change across a warming tundra biome. Nature **562**: 57–80. doi:10.1038/s41586-018-0563-7

Bond, N. A., M. F. Cronin, H. Freeland, and N. Mantua. 2015. Causes and impacts of the 2014 warm anomaly in the NE Pacific. Geophys. Res. Lett. **42**: 3414–3420. doi:10.1002/2015GL063306

Carmack, E. C., S. Vagle, J. Morrison, and B. E. Laval. 2014. Space-for-time proxy for climate change in deep lakes in the Canadian cordillera: Seasonality along a latitudinal climate gradient. J. Great Lakes Res. **40**: 608–617. doi:10.1016/j.jglr.2014.06.007

Checkley, D. M., and J. A. Barth. 2009. Patterns and processes in the California Current System. Prog. Oceanogr. **83**: 49–64. doi:10.1016/j.pocean.2009.07.028

Cullen, J. J. 1982. The deep chlorophyll maximum: Comparing vertical profiles of chlorophyll *a*. Can. J. Fish. Aquat. Sci. **39**: 791–803. doi:10.1139/f82-108

De la Cruz-Orozco, M. E., and others. 2017. Phytoplankton biomass and production off the Baja California Peninsula: 1997-2016. Cien. Mar. **43**: 217–228. doi:10.7773/cm.v4314.2793

Deutsch, C., and others. 2021. Biogeochemical variability in the California Current System. Prog. Oceanogr. **196**: 102565. doi:10.1016/j.pocean.2021.102565

Di Lorenzo, E., and N. Mantua. 2016. Multi-year persistence of the 2014/15 North Pacific marine heatwave. Nat. Clim. Change **6**: 1042–1047. doi:10.1038/nclimate3082

Dong, K., K. Ø. Kvile, N. C. Stenseth, and L. C. Stige. 2020. Associations among temperature, sea ice and phytoplankton bloom dynamics in the Barents Sea. Mar. Ecol. Prog. Ser. **635**: 25–36. doi:10.3354/meps13218

Du, X., and W. T. Peterson. 2018. Phytoplankton community structure in 2011–2013 compared to the extratropical warming event of 2014–2015. Geophys. Res. Lett. **45**: 1534–1540. doi:10.1002/2017GL076199

Eppley, R. W., A. F. Carlucci, O. Holm-Hansen, D. Kiefer, J. J. McCarthy, E. Venrick, and P. M. Williams. 1971. Phytoplankton growth and composition in shipboard cultures supplied with nitrate, ammonium, or urea as the nitrogen source. Limnol. Oceanogr. **16**: 741–751. doi:10.4319/LO.1971.16.5.0741

Eppley, R. W., F. P. Chavez, and R. T. Barber. 1992. Standing stocks of particulate carbon and nitrogen in the equatorial Pacific at 150°W. J. Geophys. Res. **97**: 655–661. doi:10.1029/91JC01386

Garrison, D. L., and others. 2000. Microbial food web structure in the Arabian Sea: A US JGOFS study. Deep-Sea Res. II: Top. Stud. Oceanogr. **47**: 1387–1422. doi:10.1016/S0967-0645(99)00148-4

Geider, R. J. 1987. Light and temperature dependence of the carbon to chlorophyll *a* ratio in microalgae and cyanobacteria: Implications for physiology and growth of phytoplankton. New Phytol. **106**: 1–34. doi:10.1111/j.1469-8137.1987.tb04788.x

Gómez-Ocampo, E., G. Gaxiola-Castro, R. Durazo, and E. Beier. 2017. Effects of the 2013-16 warm anomalies on the California Current phytoplankton. Deep-Sea Res. II: Top. Stud. Oceanogr. **151**: 64–76. doi:10.1016/j.dsr2.2017.01.005

Holm-Hansen, O., C. J. Lorenzen, R. W. Holms, and J. D. H. Strickland. 1965. Fluorometric determination of chlorophyll. ICES J. Mar. Sci. **30**: 3–15. doi:10.1093/icesjms/30.1.3

Kahru, M., M. G. Jacox, and M. D. Ohman. 2018. CCE1: Decrease in the frequency of oceanic fronts and surface chlorophyll concentration in the California Current System during the 2014–2016 northeast Pacific warm anomalies. Deep-Sea Res. I: Oceanogr. Res. Pap. **140**: 4–13. doi:10.1016/j.dsr.2018.04.007

Kintisch, E. 2015. 'The Blob' invades Pacific, flummoxing climate experts. Science **348**: 17–18. doi:10.1126/science.348.6230.17

Landry, M. R., M. D. Ohman, R. Goericke, M. R. Stukel, and K. Tsyrklevich. 2009. Lagrangian studies of phytoplankton growth and grazing relationships in a coastal upwelling ecosystem off Southern California. Prog. Oceanogr. **83**: 208–216. doi:10.1016/j.pocean.2009.07.026

Leising, A. W., and others. 2015. State of the California Current 2014-15: Impacts of the Warm-Water "Blob". CalCOFI Rep. **56**: 31–68 https://ir.library.oregonstate.edu/concern/articles/h989r499g

McCabe, R. M., and others. 2016. An unprecedented coastwide toxic algal bloom linked to anomalous ocean conditions. Geophys. Res. Lett. **43**: 10366–10376. doi:10.1002/2016GL070023

McClatchie, S., and others. 2016. State of the California Current 2015-16: Comparisons with the 1997-98 El Niño.

CalCOFI Rep. **57**: 1–57 https://escholarship.org/uc/item/730558jh

Menden-Deuer, S., and E. J. Lessard. 2000. Carbon to volume relationships for dinoflagellates, diatoms and other protist plankton. Limnol. Oceanogr. **45**: 569–579. doi:10.4319/lo.2000.45.3.0569

Monger, B. C., and M. R. Landry. 1993. Flow cytometric analysis of marine bacteria with Hoechst 33342. Appl. Environ. Microbiol. **59**: 905–911. doi:10.1128/aem.59.3.905-911.1993

Monteiro, M. R., A. J. Marshall, I. Hawes, C. K. Lee, I. R. McDonald, and S. C. Cary. 2022. Geochemically defined space-for-time transects successfully capture microbial dynamics along lacustrine chronosequences in a polar desert. Front. Microbiol. **12**: 783767. doi:10.3389/fmicb.2021.783767

Morrow, R. M., M. D. Ohman, R. Goericke, T. B. Kelly, B. M. Stephens, and M. R. Stukel. 2018. CCE V: Primary production, mesozooplankton grazing, and the biological pump in the California Current Ecosystem: Variability and response to El Niño. Deep-Sea Res. I: Oceanogr. Res. Pap. **140**: 52–62. doi:10.1016/j.dsr.2018.07.012

Ohman, M. D., K. Barbeau, P. J. S. Franks, R. Goericke, M. R. Landry, and A. J. Miller. 2013. Ecological transitions in a coastal upwelling ecosystem. Oceanography **26**: 210–219. doi:10.5670/oceanog.2013.65

Peña, M. A., N. Nemcek, and M. Robert. 2019. Phytoplankton responses to the 2014–2016 warming anomaly in the northeast subarctic Pacific Ocean. Limnol. Oceanogr. **64**: 515–525. doi:10.1002/lno.11056

Peterson, W., M. Robert, and N. Bond. 2015. The warm blob—Conditions in the northeastern Pacific Ocean. PICES Press **23**: 37–38.

Rykaczewski, R. R., and J. P. Dunne. 2010. Enhanced nutrient supply to the California Current Ecosystem with global warming and increased stratification in an earth system model. Geophys. Res. Lett. **37**: L21606. doi:10.1029/2010GL045019

Shanks, A. L., and others. 2020. Marine heat waves, climate change, and failed spawning by coastal invertebrates. Limnol. Oceanogr. **65**: 627–636. doi:10.1002/lno.1133

Sherr, E. B., and B. F. Sherr. 1993. Preservation and storage of samples for enumeration of heterotrophic protists, p. 207–212. *In* P. K. Kemp [ed.], Handbook of methods in aquatic microbial ecology. CRC Press. doi:10.1201/9780203752746

Stoecker, D. A. 1998. Conceptual models of mixotrophy in planktonic protists and some ecological and evolutionary implications. Eur. J. Protistol. **34**: 281–290. doi:10.1016/S0932-4739(98)80055-2

Taylor, A. G., and M. R. Landry. 2018. Phytoplankton biomass and size structure across trophic gradients in the southern California Current and adjacent ocean ecosystems. Mar. Ecol. Prog. Ser. **592**: 1–17. doi:10.3354/meps12526

Taylor, A. G., M. R. Landry, K. E. Selph, and J. J. Wokuluk. 2015. Temporal and spatial patterns of microbial community biomass and composition in the Southern California Current Ecosystem. Deep-Sea Res. II: Top. Stud. Oceanogr. **112**: 117–128. doi:10.1016/j.dsr2.2014.02.006

Unrein, F., J. M. Gasol, F. Not, I. Forn, and R. Massana. 2014. Mixotrophic haptophytes are key bacterial grazers in oligotrophic coastal waters. ISME J. **8**: 164–176. doi:10.1038/ismej.2013.132

Whitney, F. A. 2015. Anomalous winter winds decrease 2014 transition zone productivity in the NE Pacific. Geophys. Res. Lett. **42**: 428–431. doi:10.1002/2014GL062634

Wyatt, A. M., L. Resplandy, and A. Marchetti. 2022. Ecosystem impacts of marine heat waves in the northeast Pacific. Biogeosciences **19**: 5689–5705. doi:10.5194/bg-19-5689-2022

Xu, T., M. Newman, A. Capotondi, and E. Di Lorenzo. 2021. The continuum of northeast Pacific marine heatwaves and their relationship to the tropical Pacific. Geophys. Res. Lett. **48**: 2020GL090661. doi:10.1029/2020GL090661

Yang, B., S. R. Emerson, and M. A. Peña. 2018. The effect of the 2013–2016 high temperature anomaly in the subarctic Northeast Pacific (the "Blob") on net community production. Biogeosciences **15**: 6747–6759. doi:10.5194/bg-15-6747-2018

Zaba, K. D., and D. L. Rudnick. 2016. The 2014-2015 warming anomaly in the Southern California Current System observed by underwater gliders. Geophys. Res. Lett. **43**: 1241–1248. doi:10.1002/2015GL067550

Acknowledgments

We gratefully acknowledge captains, crews, and all CalCOFI and CCE colleagues who contributed to sample collections. Shonna Dovel collected most of the phytoplankton samples at sea; Andrew Taylor and John Wokuluk made major contributions to developing the EPI microscopy database. We thank the CalCOFI Program for availability of hydrographic and nutrient data at https://calcofi.org/. This research was supported by U.S. National Science Foundation grants OCE-0417616, OCE-1026607, and OCE-1614359 to the CCE-LTER Program and by a Mullin Fellowship from Scripps Institution of Oceanography to ALF.

Conflict of Interest

None declared.

Submitted 05 October 2023
Revised 06 March 2024
Accepted 16 June 2024

Associate editor: Katherina Petrou